P and M Class Phasor Measurement Unit Algorithms using Adaptive Cascaded Filters

A. J. Roscoe, I. F. Abdulhadi and G. M. Burt, *Member, IEEE*

***Abstract*—The new standard C37.118.1 lays down strict performance limits for phasor measurement units (PMUs) under steady-state and dynamic conditions. Reference algorithms are also presented for the P (performance) and M (measurement) class PMUs. In this paper, the performance of these algorithms is analysed during some key signal scenarios, particularly those of off-nominal frequency, frequency ramps, and harmonic contamination. While it is found that total vector error (TVE) accuracy is relatively easy to achieve, the reference algorithm is not able to achieve a useful ROCOF (rate of change of frequency) accuracy. Instead, this paper presents alternative algorithms for P and M class PMUs which use adaptive filtering techniques in real time at up to 10 kHz sample rates, allowing consistent accuracy to be maintained across a ±33% frequency range. ROCOF errors can be reduced by factors of >40 for P class and >100 for M class devices.**

***Index Terms*-- Power system measurements, Fourier transforms, Frequency measurement, Power system state estimation, Phase estimation, Power system parameter estimation, Power system harmonics, Power system stability.**

I. Nomenclature

f	frequency (actual) (Hz)
f_M	frequency (measured) (Hz)
f_F	frequency (feedback to quadrature oscillators and filters) (Hz)
f_0	nominal frequency (Hz)
f_C	Basic M class filter 3dB cutoff frequency
f_{Mix}	Mixing frequency (wanted) from Fourier correlation
F_{ADC}	Sample rate of the ADCs, and computational frame rate
F_S	reporting rate (Hz)
Φ	phase (rad)
Φ_Q	quadrature oscillator phase (rad)
L	filter length (cycles)
N	filter order
ROCOF	Rate of change of frequency (Hz/s)
S	number of samples per cycle at f_0
T	Total filter window length (s)
t	time (s)
W_k	filter weights

The authors acknowledge the funding and support provided by Rolls-Royce PLC under the UTC (University Technology Centre) programme.

The research leading to the results described in this paper was partially funded by the European Metrology Research Program (EMRP), which is jointly funded by the EMRP participating countries within EURAMET and the European Union on the basis of Decision No 912/2009/EC.

A. J. Roscoe I. F. Abdulhadi and G. M. Burt are with the University of Strathclyde, Glasgow, G1 1XW, UK. (phone: +44 (0)141 548 2951; fax +44 (0)141 548 4872; e-mail: andrew.j.roscoe@strath.ac.uk).

II. Introduction

PHASOR measurement units (PMUs) are being deployed in ever increasing numbers. They can be used to determine system instability [1, 2], detect disconnected lines and islanded sections [3], aid in power system restoration [4], and to enable state estimator algorithms to converge with higher accuracy [5-7]. However, testing of early PMUs showed a large disparity between the reported values from PMUs provided by different manufacturers, particularly when frequency was off-nominal, during dynamic events, and when harmonic/inter-harmonic content was present [8, 9]. Even the 2005 version of the PMU standard IEEE C37.118 (2005) [10] left ambiguity in the required response to dynamic changes and the exact definition of vector/timestamp relationships [6, 11, 12].

A new standard has been published as IEEE C37.118.1 (Measurements)[13] and IEEE C37.118.2 (Data Transfer)[14]. This lays down strict requirements for the required response to dynamic events, and harmonic/inter-harmonic signal content. The required TVE (Total Vector Error) accuracy is still 1%, although 0.4% is desirable [5]. It also specifies accuracy requirements for frequency and ROCOF (rate of change of frequency) measurements. The relationships between measurement windows, reported timestamps, and latency are all described. Furthermore, a "Basic synchrophasor estimation" algorithm is provided, with the implication that it will be compliant if implemented correctly. Testing of PMUs will be possible using new processes produced under the EMRP EURAMET programme [15].

In [16] a P class version of the Basic algorithm was compared to an improved algorithm with adaptive filtering. This showed that the Basic P class algorithm can easily comply with the TVE specification, but that its frequency and ROCOF errors are excessive for the off-nominal frequency cases containing harmonics. The adaptive filter algorithm performed much better, achieving ROCOF errors of <0.1 Hz/s even with a total harmonic distortion (THD) as high as 28%.

In this paper, [16] is extended to encompass both P and M class devices and filters, presenting algorithms which perform much better than the Basic algorithm and showing results comparing the outputs. The M class device is significantly more complex than the P class device, since the filtering is variable length and there are greater requirements to filter inter-harmonic signals. The proposed algorithm differs from most published enhancements to DFT-based measurements in

that the fundamental filtering is altered, rather than pre-adjusting the samples or post-adjusting the measured values. This leads to a cleaner and more flexible implementation, with minimal computational effort.

III. The Importance of Frequency and ROCOF

While compliance with the TVE specification is relatively easy, compliance with the frequency and ROCOF requirements is much more problematic. This is particularly the case at off-nominal frequencies under the influence of harmonic content, since any unwanted signals emerging from the filters will impart ripple onto the measured signal phase. While this ripple may be small enough to still be compliant with the TVE requirement, the frequency is calculated by:

$$f = \frac{1}{2\pi}\frac{d\Phi}{dt} \tag{1}$$

where Φ is the measured phase. Thus even tiny amounts of ripple or noise on the measurement of Φ can cause large ripple or noise on the measurement of frequency. The problem is further compounded for the measurement of ROCOF, since:

$$ROCOF = \frac{df}{dt} = \frac{1}{2\pi}\frac{d^2\Phi}{dt^2} \tag{2}$$

Frequency and ROCOF measurements are important because the PMU measurements are only useful when compared with each other at a Phasor Data Concatenator (PDC). However, the timestamps from the many PMUs will vary, due to their different classes, reporting rates (measurement windows), and variable data transfer times. A P-class device might report at a rate F_S =50 Hz, i.e. every 20ms, with the timestamps ~20ms prior to the reporting instants due to the window length of 2 cycles. However, an M-class device with F_s=10 Hz will report only every 100ms, with the timestamp 250-300ms prior to the reporting instant [13]. Data transfer time through a network (i.e. Figure 2 in [14]) might also vary between zero and 30-50ms [2, 6, 17].

The total spread of timestamps received at the PDC from all PMUs could therefore be over a range of 10 to 300ms (or more) into the past. The PDC needs to decide a common time point t_C, and normalise all reported PMU phases to this instant in time, with an equation such as:

$$\Phi = \Phi_{reported} + 2\pi\left(\Delta t\left(f_{reported} - f_0\right) + \frac{(\Delta t)^2}{2} ROCOF_{reported}\right) \tag{3}$$

where

$$\Delta t = t_C - t_{reported\_timestamp} \tag{4}$$

If t_C is set to the present time, then Δt could be up to 70ms for a P-class PMU, or up to 300ms for an M-class PMU. If a TVE of 1% is to be maintained, then the error in Φ must be less than 0.01 rad. Limits on the acceptable accuracies of both reported frequency and ROCOF can be obtained from (3) by holding one of them at zero and solving (3) to find the other, for given values of Δt and the 0.01 rad phase error. These limits are shown in TABLE I. Both will need to be less than these figures, since each corresponds individually to a TVE of 1% and in practice both errors may occur together.

It is interesting to compare these limits with the steady-state specifications given in Table 4 of C37.118, which are also shown in TABLE I. The specified ROCOF accuracy of 0.01 Hz/s at steady-state, off-nominal frequency, under the influence of harmonics is actually very difficult or impossible to achieve from a P class device (as will be shown). However, TABLE I suggests that perhaps there is no real need to achieve 0.01 Hz/s from P class devices.

TABLE I
Frequency and ROCOF errors leading to 1% TVE errors at the PDC, compared to C37.118 specifications

	P class Δt=80ms	M class, F_S=50 Hz Δt=100ms	M class, F_S=10 Hz Δt=300ms
Frequency error limit leading to 1% TVE error at the PDC	0.022 Hz	0.016 Hz	0.0053 Hz
Steady-state frequency error specification, Table 4 of C37.118	0.005 Hz	0.025 Hz	0.005 Hz
ROCOF error limit leading to 1% TVE error at the PDC	0.65 Hz/s	0.32 Hz/s	0.035 Hz/s
Steady-state ROCOF error specification, Table 4 of C37.118	0.01 Hz/s	6 Hz/s	2 Hz/s

For M class, the steady-state requirements for frequency accuracy appear to be in the right region, although 0.025 Hz for the F_S=50 Hz device is perhaps double the value that it should usefully be. The requirements for ROCOF accuracy are far too loose to be useful at the PDC or for power system control.

The new standard makes no mention of unbalance, and restricts harmonics to 1% (P class) and 10% (M class), a single harmonic at a time, while frequency f is constant. In real scenarios, many harmonics may be applied simultaneously while f changes, and an expectation that a P class PMU will only be exposed to a single harmonic at 1% magnitude is unrealistic, particularly within low-voltage networks where THD can reach 8% and be compliant with [18].

IV. PMU Algorithms and Background

A. The Basic algorithm from C37.118

The single-phase section of the Basic algorithm for a PMU described in C37.118.1 is shown in Fig. 1 and Fig. 2, and follows principles suggested in [19]. In the Basic architecture, the input signals are correlated with quadrature waveforms at the nominal frequency f_0. The ideal output of each single-phase section is a single fundamental phasor, each of which has a magnitude proportional to the voltage on each phase, and a phase which rotates at a rate of $2\pi(f-f_0)$.

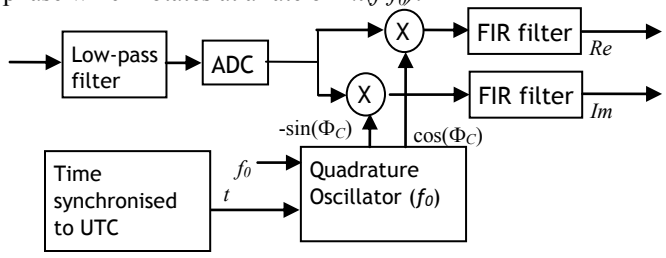

Fig. 1. Single-phase section of the Basic PMU

This is a slightly expanded postprint of a paper published in IEEE Transactions on Power Delivery [http://dx.doi.org/10.1109/TPWRD.2013.2238256] and is subject to IEEE copyright.

During normal operation, the phase angles of the $\mathbf{V_a}$, $\mathbf{V_b}$, and $\mathbf{V_c}$ phasors are separated by approximately 120°. The overall positive-sequence phasor can be calculated by:

$$\mathbf{V^P} = \mathbf{V_a} + \mathbf{V_b}e^{\frac{2\pi}{3}j} + \mathbf{V_c}e^{-\frac{2\pi}{3}j} \quad (5)$$

Assuming that the single-phase sections are effective at filtering out noise, harmonics, etc. from $\mathbf{V_a}$, $\mathbf{V_b}$ and $\mathbf{V_c}$, then $\mathbf{V^P}$ will also rotate at a steady rate of $2\pi(f-f_0)$, for steady state inputs.

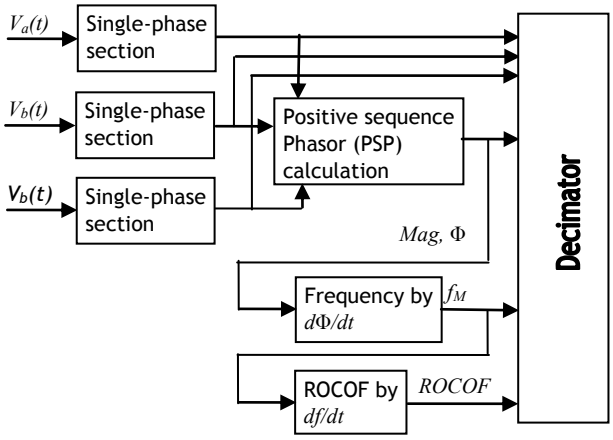

Fig. 2. Three-phase "Basic" PMU

1) Recommended P class filter

In the Basic P-class algorithm, the FIR (Finite Impulse Response) filter used is a fixed-length triangular-weighted symmetric filter of length 2 cycles, designed to work optimally at the nominal system frequency f_0. The filter produces notches with high attenuation at every multiple of f_0, which are useful to attenuate contamination due to harmonics. Equations to design the filter are given in [13], and an example is shown in Fig. 3.

the filter weights are determined by:

$$W_k = \left(1 - \frac{2}{(N+2)}|k|\right) \quad (6)$$

where:

$$k = -\frac{N}{2}, -\frac{N}{2}+1, \ldots . \frac{N}{2},$$

and N = filter order, where $N=2(S-1)$ and S is the number of samples per cycle at nominal frequency f_0.

An example is given in [13] for a filter with 15 samples per cycle, giving an order 28 FIR filter. This is reproduced below:

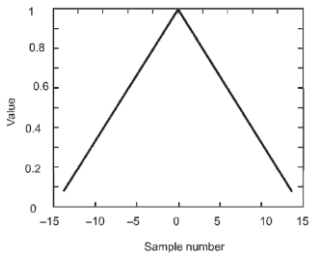

Fig. 3. P class FIR filter coefficient weights (29 off) for S=15 samples/cycle and order N=28 [13]

Since the filter is symmetric ("zero phase") the timestamp of the measurement can be allocated to a point exactly half-way through the FIR filter time window.

There are 2 problems with such an implementation, both of which are identified in [13]. The problems become evident when the mixing frequencies are considered. The mixing frequencies appear at the inputs to the FIR filters in Fig. 1. If frequency is nominal, i.e. $f=f_0$, then the mixed signal consists of the dominant (wanted) DC component, plus unwanted components at $f+f_0=2f_0$:, and at every frequency $f_H=f_0\pm Hf_0$ for the harmonics where H>1 and $H \in N$. However, when $f\neq f_0$ the wanted component is no longer at DC, but is present at $f_{Mix}=|f-f_0|$ Hz. The unwanted harmonic components also shift from $f_H=f_0\pm Hf_0$ *to* $f_H=f_0\pm Hf$.

1) For off-nominal frequencies, the FIR filter notches no longer correspond exactly to the unwanted frequencies in the mixed signal. Therefore, the ability of the FIR filter to reject harmonic contamination reduces as frequency diverges from nominal [20-23]. This is the "leakage" and "picket fence" problem in conventional DFTs and FFTs.
2) While the Basic FIR filter is carefully designed to be symmetric and "zero phase", it has a finite amplitude attenuation of the wanted component when $f\neq f_0$, i.e. the mixing frequency f_{Mix} is not 0 (DC) but is finite. Therefore, the measured amplitude needs to be calibrated.

It would, in theory, be possible to address 1) by carefully designing new filters (in real time) to place notches at the desired frequencies using, for example, the Tustin transformation [24] or other mathematical methods. However, designing the FIR in this manner is likely to be a time-consuming process. Also, it (alone) does not address 2).

2) Basic M class filter

The recommended filter for the M class algorithm is a fixed-weight FIR filter of substantially greater length than the 2-cycle P class filter. The filter has a defined pass-band and stop-band, and is of the "brick wall" design (Fig. 4). The pass-band has ideally a flat (or at least characterisable) amplitude response across a frequency range defined by the deviation $|f-f_0|$ which the algorithm must cope with. This is 2 Hz for the longest M class filter (F_S=10) and 5 Hz at the highest, and limits the useful frequency range of the Basic algorithm to these figures. The stop-band should have at least 20dB attenuation, to attenuate both harmonics and inter-harmonics which might appear at mixing frequencies close to 0 Hz if the hardware anti-aliasing filters are not effective.

This is a slightly expanded postprint of a paper published in IEEE Transactions on Power Delivery [http://dx.doi.org/10.1109/TPWRD.2013.2238256] and is subject to IEEE copyright.

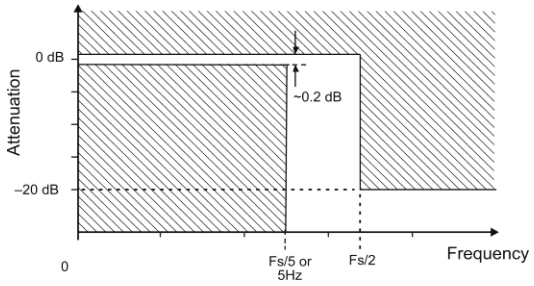

Fig. 4. Basic M class filter frequency response mask [13]

Suitable filter orders, cutoff frequencies, and the equation to calculate filter weights are given in [13] section C.6. By fitting curves to the data in [13] Table C.1 using simple Excel tools, the following approximate empirical equations can be deduced, which allow Basic M class filters to be designed for arbitrary sample rates, reporting rates, and nominal frequencies:

$$L_{M\_Basic} = \left(\frac{f_0}{F_S}\right) \times \left(5.8943 + 1.467 \ln\left(\frac{f_0}{F_S}\right)\right) \quad \text{cycles} \tag{7}$$

$$N_{M\_Basic} = L_{M\_Basic}\left(\frac{F_{ADC}}{f_0}\right) \quad \text{(filter order)} \tag{8}$$

$$f_{M\_Basic} = F_S(0.1967 - 0.0003F_S) \approx \frac{F_S}{5} \quad \text{Hz} \tag{9}$$

where L is the filter length in cycles, N is the order, and f_{M_Basic} is the filter "reference" frequency. Examples of these filters are shown later in section V. B. . The Basic M class filter makes no attempt to put notches at frequencies which correspond to mixing frequencies caused by harmonic signals. The filter is symmetric, and so maintains its "zero phase" property if the mixing frequency is constant.

B. Other proposed PMU algorithms

There are several algorithms which could be used within PMUs. The different approaches are driven by the problems of dealing with off-nominal frequency which leads to leakage and picket-fence effects in conventional DFT/FFT algorithms such as the Basic algorithm [22, 23], in coping with the computational burden of the algorithms, and in dealing with DC or harmonic components. Most literature (e.g. [20]) implies that adjustment of the entire core DFT/FFT/filtering to remove the source of the leakage effects is not possible with available computing power. Consequently, literature tends to focus on pre and post-processing methods, or adjustment of sample rates.

Pre-processing methods include [21] which re-sample the data using splines and recreates an artificial signal which is always at the nominal frequency f_0. This allows the following DFT and filtering to work optimally. The drawback is that a sparse but square matrix needs to be generated and manipulated every computational frame, and the matrix dimension is roughly equal to the number of samples per cycle which could reach 200 for a PMU sampling at 10kHz. Another pre-processing approach is to use an FFT after resampling the data onto a rate which is an exact multiple of the fundamental frequency to minimise leakage, using Sine/Cosine [25] or polynomial [26] interpolation. These can be coded efficiently [27] without using variable frame rates. A full FFT is not required for a PMU, so instead a DFT could be incorporated.

A different approach is to use conventional DFT algorithms but then perform post-processing. E.g. [28] uses least-squares techniques (proposed in [19]), with a high computational burden that can be mitigated using lookup tables. In [20], equations are used to calculate accurate estimates of the fundamental, but since the DFT is conventional the harmonic rejection does not adapt to off-nominal frequencies.

Some techniques completely avoid the use of FIR filters, leading to low memory and computational requirements. However the algorithm of [29] becomes numerically unstable at high sample rates or when using less than 64-bit arithmetic. Resonant filters [30] have narrow pass-bands which makes PMU-grade accuracy difficult to achieve.

In contrast to all the above methods, in this paper we show how the core of a conventional DFT and its subsequent PMU filter(s) can be adjusted in real-time with minimal computational effort, so that neither pre nor post-processing is required to obtain harmonic rejection and accurate results over wide frequency ranges of at least a ±33%, at achievable sample (and reporting) rates of 10kHz or more.

V. The Proposed Algorithms

A. Proposed algorithm design overview

This section presents algorithm variants for P class and M class PMUs. For each of the 2 classes, there are two algorithm variants presented, TickTock and Asymmetric. All resemble the Basic algorithms, with the following major exceptions:

1) The measured frequency f_M is fed back as f_F and used to adjust the frequency of the quadrature oscillator sine and cosine signals used for the Fourier correlation.
2) The P-class filter is adjusted in real time to always place notches at frequencies which are multiples of f_F.
3) The M class filter is redesigned entirely so that it always places notches at frequencies which are multiples of f_F, while still fulfilling the low-pass filter requirements.
4) The calibration factors are customised, with particular care needed for the phase and timestamp calculations.

The algorithm designs have been developed following several years of foundation work by the authors, in the field of Fourier measurements of fundamental signal amplitude/phase and frequency. Firstly in [31] a Frequency-Locked-Loop was designed which bears some similarities to the Asymmetric algorithm variant presented below. During this work, the extensive use of cascaded exact-time averaging was recognised and used, since it allows notches to be placed at harmonic frequencies in a dynamic manner when frequency is varying, without the need to explicitly calculate filter weights. Spectral leakage and "picket fence" problems are eliminated using this filtering approach [27]. The practical implementation of such filters required careful coding implementation and optimisation to minimise execution time [32]. More recently,

the techniques were adapted for use within P class PMUs [16], in which the filter is relatively simple and fixed by the standard. During this work another approach to deal with varying frequency (the TickTock variant) was first proposed, since if offers a more tightly defined dynamic response to frequency changes than the Asymmetric variant. Now, in this paper, the work has been significantly extended to the realm of M class PMUs. These are much more complex, since there are many possible (long) filter designs, and the effect of frequency chirps during the long filters becomes significant and must be accounted for, whereas it could be ignored for the P class devices.

An overview of the proposed algorithms is shown in Fig. 5. This represents all 4 types of proposed PMU algorithm. For P class devices, the sections labelled "M Class filter x x" are bypassed. For M class devices, the section labelled "Average over 3 cycles (P class only)" is bypassed. There are other subtle differences in the implementations, particularly with respect to the calibrations, described in the text.

The initial Fourier correlation is always done by passing the Sine and Cosine path data (the "real" and "imaginary" components) through a cascaded pair of single-cycle averaging/integrating filters. For P class, this is the entire filter, and the proposed filter is identical to the Basic filter when $f=f_0$. However, the averaging/integrating filters perform their calculations over exactly one cycle period each, with the time period set by $1/f_F$, where the feedback frequency f_F follows the measured frequency f_M. The resulting filter passes the wanted signal (mixed at $f_{Mix}\approx 0$ Hz), but places notches at every multiple of f_F until the frame rate F_{ADC} is approached, thereby rejecting the unwanted fundamental mixing product at $2f_F$ and unwanted harmonics at other multiples of f_F. A simple example with f_F set to 50 Hz and a relatively low F_{ADC} is shown in Fig. 6.

The low-level software to carry out this averaging/integrating operation is described in detail in previous papers [16, 27, 31-33] so is not repeated here. The averaging/integrating algorithms are relatively memory-hungry, since each one normally requires three memory buffers, each the length of the averaging time window, to ensure integrator windup does not occur [33].

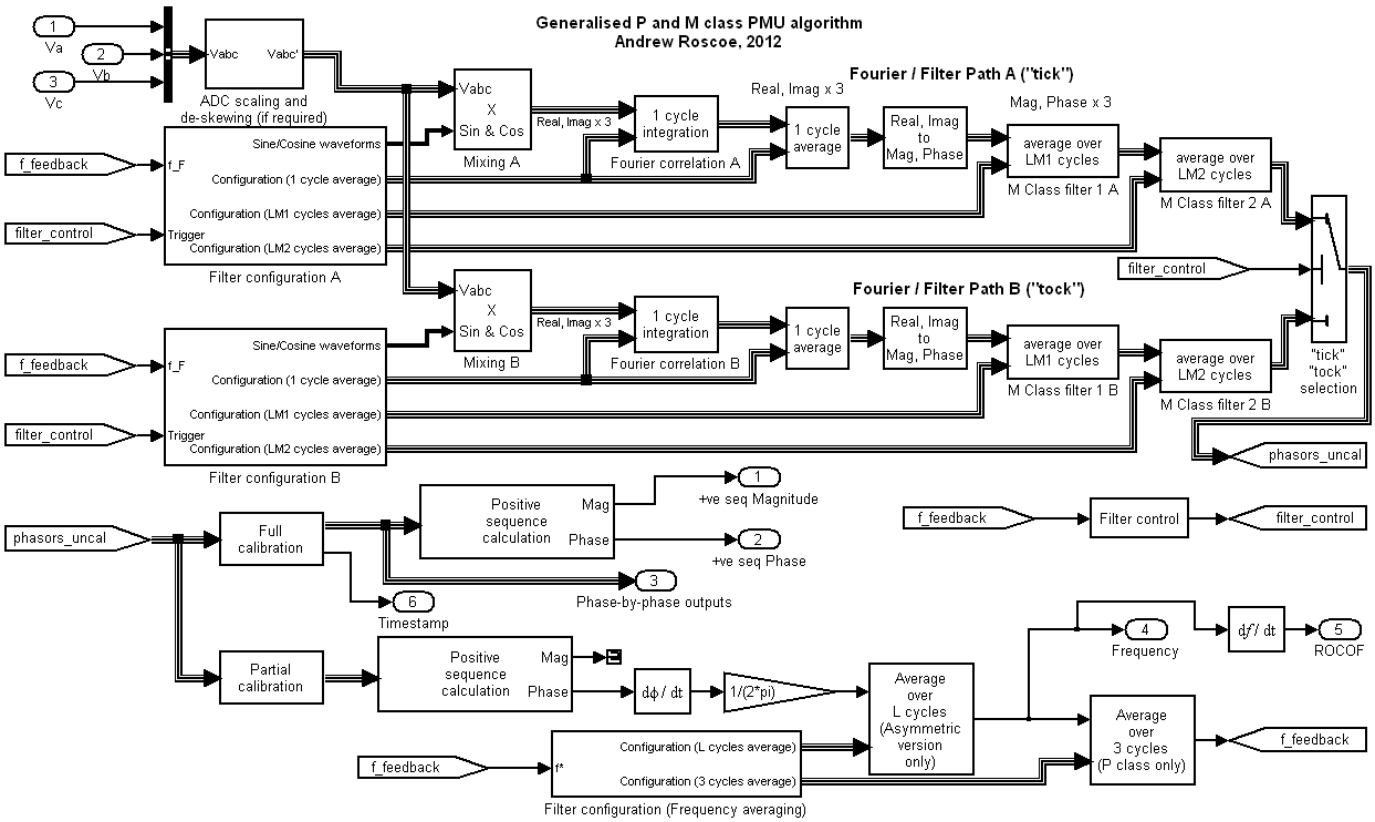

Fig. 5. High level generalised overview of the proposed algorithms

In the special case of algorithms to average phase, an extra buffer is required to cope with phase unwrapping, requiring (normally) 4 buffers for each phase averaging stage. However, contrary to the statements made in [20], these blocks can be extremely fast to execute, since only the samples at the beginning and end of the FIR filter window need to be considered in the calculations every computational frame, and each memory buffer takes only about 0.2µs or less to execute if it is carefully coded. This contrasts with a traditional FIR filter with variable weights W_k where the entire convolution needs to be carried out across the filter window every frame.

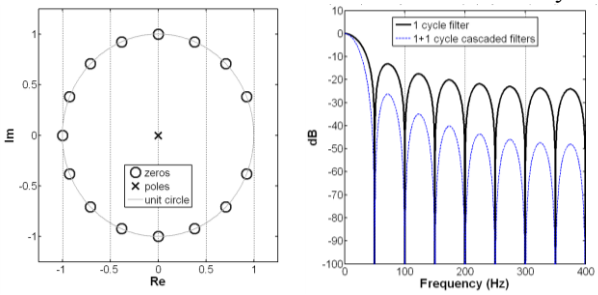

Fig. 6. Example of zeros, poles and response for 2 cascaded single-cycle averaging filters (0.02s window length per filter, 800 Hz sampling)

The P class filter has an easily defined amplitude response for non-zero mixing frequencies, given by the convolution of 2 averaging (rectangular window) filter responses in the time domain, and these can be multiplied in the frequency domain:

$$Gain_{P\_Class\_Filter} = \left(\mathrm{sinc}\left(\pi \cdot T_{1cycle} \cdot f_{Mix}\right)\right)^2 \qquad (10)$$

In the Basic algorithm, the quadrature oscillator frequency is fixed at f_0. Therefore, the mixing frequency $f_{Mix}=|f-f_0|$ could reach 2 Hz (P class) or even 5 Hz (M class with F_S>25 Hz) within the requirements [13], leading to relatively large amplitude corrections in (10) of up to ~3%.

However, for the proposed algorithms, f_{Mix} is constantly tuned towards zero. The largest expected deviation will be for a 1 Hz ROCOF, and a total frequency feedback filter length of about 5 cycles (100ms), so f_{Mix} should never be greater than about 0.1 Hz. Thus the maximum deviation of the filter gain from unity by (10) is only of the order of $1.3\text{x}10^{-5}$ (0.0013%).

B. Extension to M class

For the proposed M class devices, the overall filter length, in this paper, is set to:

$$L_M = \left(\frac{f_0}{F_S}\right) \times 5 \quad \text{Cycles} \qquad (11)$$

It can be seen by comparing (11) with (7) that the proposed M class filter is shorter than the Basic M class filter, and this could lead to a faster response time, although the distribution of actual filter weights is as important to the response time as the total filter length.

In the Basic M class design, the recommended filter (Fig. 4) needs to have a flat pass-band (±0.2dB) to F_S/5 or 5Hz, because the wanted mixing frequency will be non-zero for off-nominal frequencies. This is achieved using a Butterworth-style "brick wall" filter. In the proposed design, the maximum

mixing frequency during a 1 Hz/s ROCOF will occur with the longest filter (F_S=10 Hz, filter length 0.5s) and will be about f_{Mix}=0.5 Hz. Therefore, the pass-band does not need to be constrained to a flat response over such a wide frequency range to F_S/5 or 5Hz, but only to about 0.5 Hz. However, this would still present a problem if the entire M class filter was implemented using cascaded (convoluted) rectangular filters operating on the real/imaginary pairs, which would have amplitude responses (for steady-state frequencies) given by the product of sinc functions similar to (10), with significant attenuation, potentially greater than 0.2 dB. Also, the attenuation would be almost impossible to characterise for chirping signals with frequency varying over the duration of the filter length.

Therefore, to create the M class filter, the initial 2-cycle P class correlation output is instead transformed to a magnitude/phase pair and further filtered in a FIR filter of total length (L_M-2) cycles. The transformation of the data from real/imaginary to a magnitude/phase pair means that there is no attenuation of the wanted signal within the (L_M-2) cycle averaging sections, no matter how long the averaging period, even for chirping signals and those with ROCOF. The response to phase is similar, except that careful consideration needs to be given to phase wrapping.

This means that the gain of the overall filter from the perspective of the large wanted signal (during steady-state operation or frequency ramps with constant ROCOF) is actually that of the P class filter which is extremely flat near 0 Hz. For f_{Mix}=0.5 Hz, (10) gives a maximum gain deviation from unity of about $3.3\text{x}10^{-4}$ which can be accounted for in calibrations, but can almost be ignored, so long as the PMU is still tracking frequency. For these reasons, while Fig. 7a appears to show that the proposed M class filter is not compliant with the mask for flatness, its practical performance during operation is actually almost completely flat to within 0.033%, or 0.003 dB, which is much smaller than the standard's flatness of 0.2 dB. However, the gain of the filter from the perspective of interfering higher-frequency low-level remnants can be extremely low (Fig. 7). Effectively, the requirement for a flat pass-band has been removed, and by the removal of this constraint the entire filter design can instead be optimised to provide harmonic and inter-harmonic signal attenuation.

It is important to perform low-pass filtering in order to meet the M class PMU specifications for close-in out-of-band (OOB) signals. The filter length of the initial P class section is 2 fundamental cycles. This leaves a total time length of (L_M-2)=5(f_0/F_S)-2 fundamental cycles remaining. Firstly it makes sense to place a notch at $F_S/2*(f_F/f_0)\approx F_S/2$, thereby guaranteeing 20dB attenuation at F_S/2 as the mask of Fig. 4 requires. This is done by allocating the 1st M-class averaging filter a length of:

$$L_{M1} = \left(\frac{f_0}{F_S}\right)\times 2 \quad \text{cycles (at } f_F\text{)} \tag{12}$$

This leaves a time of 3(f_0/F_S)-2 fundamental cycles remaining. This time length could be split into many smaller cascaded sections of equal or varying length(s), providing little extra attenuation at low frequencies but significant attenuation at higher frequencies through coincident notches. However, as the results in section VI. demonstrate, the largest measurement errors arise due to the close-in OOB signals, which require filtering at the lowest frequencies. This clearly places the priority on placing an extra notch as close as possible to the low frequency F_S/2 (and every multiple of this) rather than placing many coincident notches at higher frequencies (and multiples). For this reason, the remaining filter length is used to apply a single (2nd) M-class averaging filter of length 3(f_0/F_S)-2 cycles i.e.:

$$L_{M2} = L_M - 2 - L_{M1} \quad \text{cycles} \tag{13}$$

This single filter offers the lowest frequency notch possible from the remaining filter length, at a frequency which ranges from ~F_S/2.6 for the F_S=10 Hz PMU, to ~F_S for the F_S=50 Hz PMU.

The overall frequency response is shown in Fig. 7. An example of the overall filter weights is shown in Fig. 8, although the weights themselves are not usually calculated but result from the cascaded averaging filters.

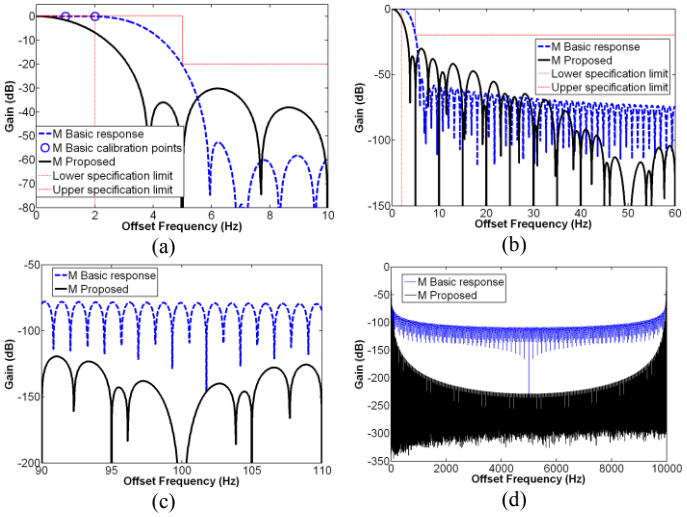

Fig. 7. Proposed adaptive M class filter compared to Basic filter, F_S=10 Hz. (a) to (d) show different frequency ranges to highlight the differences. The response shown for the proposed filter is the response to the unwanted small signals. The response to the wanted signal is essentially flat near 0 Hz.

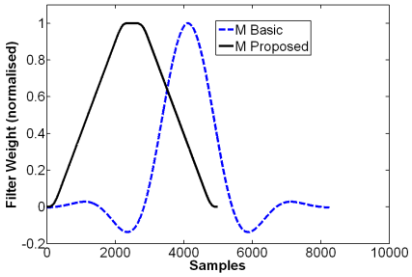

Fig. 8. Proposed adaptive M class filter weights compared to Basic filter. F_{ADC}=10 kHz, f_0=50 Hz, F_S=10 Hz, L_M=25 cycles. TickTock algorithm variant

Filter lengths differing from (11) could be examined, although filter lengths much longer or shorter than (11) are unlikely to meet both response and attenuation requirements. If

the length of the M class filter could be extended to $6(f_0/F_S)$ without violating response time requirements, this would have benefits for OOB signal attenuation. This is particularly true for the F_S=50 Hz PMU since it would allow two coincident notches at $F_S/2$ to be placed. Initial comparison of the proposed filters (their weight distributions) against the Basic filter for F_S=10 Hz (Fig. 8) and F_S=50 Hz [34] suggests such longer filters would probably exceed the required response times, but this has not yet been confirmed through formal testing. Filters with non-integral cycle lengths are possible, although integer cycle lengths are favoured since they always place notches at every harmonic.

C. TickTock algorithm variant

Two variants of algorithm are presented, both for P and M class. These variants are TickTock and Asymmetric, first introduced in [16]. The TickTock variant uses a duplicated pair of filter paths at the high level, shown on Fig. 5 as "Path A (tick)" and "Path B (tock)". Each filter path and quadrature oscillator is used in turn, with each path set to a piecewise-fixed oscillator frequency f_F and matching filter configuration for the duration of its use. The advantage of this is that the filter performance is still "zero phase" (and characterisable) when ROCOF=0. Regular changeovers are triggered between the filter paths A and B so that f_{Mix} remains small and the filter notches are kept well aligned with the mixed harmonics from the quadrature correlation.

The smallest interval which can be used is equal to the total FIR filter length (2 cycles for P class and L_M cycles for M class). This time interval allows each FIR filter path to be configured to the new frequency, and to accumulate a full set of data before it is then actively used. Compared to the implementation in [16], in this paper the low-level averaging algorithms required in the filter paths were slightly simplified since the high-level use of a TickTock arrangement removes the need to cope with integrator windup and phase wrapping of large angles within the low-level blocks. This reduces the low-level memory requirement and computation burden of the TickTock algorithm from that described in [16]. Specifically, the number of memory buffers is reduced from 3 [33] to 2 for normal averaging operations, and from 4 to 2 for averaging of phase.

Placement of the timestamp can be done easily, because the length of the filter window in use is 2 cycles (P class) or L_M cycles (M class) times $1/f_F$, where f_F is the piecewise-fixed oscillator frequency and filter configuration in use at any time.

$$t_{Timestamp} = t_{Now} - \frac{T}{2} \tag{14}$$

where $t_{Timestamp}$ is the reported timestamp, and t_{Now} is the time of the most recent ADC (analogue to digital converter) sample and calculation. Also, when the signal phase is calibrated, this time offset must be accounted for by an equation such as:

$$\Phi_{Timestamp} = \Phi_{Uncalibrated} + \Phi_Q - 2\pi f_F\left(\frac{T}{2}\right) - 2\pi f_0\left(t_{Now} - \frac{T}{2}\right) \tag{15}$$

where the uncalibrated measurement phase and oscillator phase Φ_Q are the most recent values obtained in real time at time t_{Now}. The true values of amplitude and phase also need to be calibrated due to known responses of any analogue components such as instrumentation and anti-aliasing filters. For the TickTock algorithm, an additional phase calibration is required during ROCOF events (described in section V. D.).

All these calibrations are applied in the "Full calibration" block shown on Fig. 5. On this figure, a second block called "Partial calibration" is shown in the path which determines frequency and ROCOF measurements. This block omits the phase calibrations due to instrumentation and ROCOF chirp response (see below), as it is found that including such factors in the closed-loop frequency path can lead to oscillation/ringing, but does not improve accuracy.

D. Frequency chirp due to ROCOF and phase calibration for the TickTock algorithm

During frequency ramps, ROCOF is finite and the signal from the Fourier correlation (going into the filter) becomes a frequency chirp for the M class Basic and TickTock algorithms which have fixed quadrature oscillator frequencies over the filter window periods. In the case of the Basic M class filter, the effect is hard to quantify since the FIR filter averages the signal as a vector in a real/imaginary pair, and for a frequency chirp the response is difficult or impossible to characterise, being much more complex than the simple steady-state frequency response shown in Fig. 4. For the proposed TickTock algorithm however, the long filters average magnitude/phase, and therefore the response of the phase-averaging part is easy to characterise. For example:

$$\Phi_{actual} = \Phi_{timestamp} + 2\pi f t + \pi(ROCOF)t^2 \tag{16}$$

The phase measurement inside the PMU is made by averaging the values of Φ over the filter window which spans a range of $-T/2$ to $+T/2$ s from the timestamp where Φ, f and ROCOF are estimated. This averaging is done (for P class PMUs) over a triangular window:

$$\begin{aligned} w(t) &= 1 + \frac{2t}{T} \quad -T/2 \le t \le 0 \\ w(t) &= 1 - \frac{2t}{T} \quad 0 < t \le -T/2 \end{aligned} \tag{17}$$

So the averaging reveals:

$$\Phi_{measured} = \frac{\int_{-T/2}^{T/2}\left(\Phi_{timestamp} + 2\pi f t + \pi(ROCOF)t^2\right)w(t)\cdot dt}{\int_{-T/2}^{T/2} w(t)\cdot dt} \tag{18}$$

which evaluates as:

$$\Phi_{measured} = \Phi_{timestamp} + \frac{\pi(ROCOF)T^2}{24} \tag{19}$$

i.e. there is a phase correction of

$$\Phi_C = k\frac{\pi(ROCOF)T^2}{24} \quad \text{rad} \tag{20}$$

where k=1 for a triangular window. The correction factor could be used for the P class TickTock PMU but note that in this case, T≈0.04 s (2 cycles) and even at 1 Hz/s, the correction

only accounts for 0.01°. However, for the M class devices T can be as large as 0.5 s when F_S=10. In this case the correction is up to 2° for a 1 Hz/s ROCOF and this is significant.

In practice, for an M class filter, the factor k in (20) is not exactly 1 because it can be seen from Fig. 8 that the proposed M class filter is not perfectly triangular, due to the cascaded use of 4 filters. The approach taken in this work was to characterise the required value k for different filter lengths by applying frequency ramps and tuning k to obtain the best TVE accuracy from the PMU, finding:

$$k = 0.3806 + 0.0252 L_M - 0.0003 L_M^2 \quad (21)$$

which, for example, gives values of 0.5 for L_M=5 and 0.85 for L_M=25. A more theoretical approach could be taken, by examining the actual filter weights resulting from the cascaded filters, and repeating the process of (17)-(20) using numerical integration techniques. This would be done off-line, in advance, and not in real-time due to the complexity of the operation. The values of k could be stored in a look-up table.

E. Asymmetric algorithm variant

The second algorithm variant is called Asymmetric and requires only the "Path A" filter path shown in Fig. 5. However, the memory requirements and computational burden are similar to the TickTock variant, due to additional filters and buffers required in the Asymmetric variant, versus the simplifications to the lower-level TickTock algorithms previously described. In this algorithm, there is no deliberate attempt to maintain the "zero phase" symmetric nature of the filter, although it will be so when ROCOF=0. However, the use of magnitude/phase averaging in the M class filter means that the problems of asymmetry are significantly reduced.

Because there is only one filter path, the quadrature oscillator frequency f_F constantly changes in real-time to track the measured frequency f_M, and the filters are constantly reconfigured likewise so that the notches fall at the desired locations. The drawbacks are that the timestamp and phase calibrations (14) & (15) are no longer valid. Instead the value of oscillator phase Φ_Q which was in use at the timestamp can instead be pulled back from a memory buffer of a length exactly equal to T/2, using linear interpolation if necessary. During ROCOF events this process automatically compensates for the dominant portion of the frequency chirp effects and so calibration (19) is not required.

A feature of this algorithm is that there is a continuous feed-forward effect within the frequency and ROCOF calculations. This is because the value of the quadrature oscillator phase Φ_C is incremented every computational frame by $2\pi f_F/F_{ADC}$, so during constant ROCOF frequency ramps, the frequency $2\pi d\Phi_Q/dt$ moves up at the same ROCOF as the actual frequency f. Thus there is essentially no latency in the initial frequency measurement during times that ROCOF is constant. (But during changes in ROCOF, there is the expected latency). Consequently, to generate a measurement of frequency which is accurate at the timestamp, for constant-ROCOF situations, the frequency measurement needs to be delayed by T/2. More usefully, this "spare time" can be used to apply a further averaging over exactly 2 cycles (for P class) or L_M cycles (for M class). This reduces general noise, and the averaging over exactly an integer number of cycles places further yet filter notches at all multiples of the measured frequency.

F. Memory requirements and execution speed

The memory required for the Basic and proposed algorithms is dominated by the FIR filter and averaging/integrating buffers. Requirements for P class devices are relatively small. Requirements for the M class devices are much larger, and are given in TABLE II.

TABLE II
APPROXIMATE MEMORY REQUIREMENTS FOR M CLASS PMUS

	Memory requirement (bytes)	Example M class with F_S=10 Hz
Basic	$\frac{B \cdot F_{ADC} \cdot P_3 \cdot V_2 \cdot L_{M\_Basic}}{f_0}$	0.47 MB
Symmetric "tick-tock"	$\frac{B \cdot F_{ADC}(P_3 P_2)(V_2 A_2 L_2 + (A_2 + AP_2)(L_M - L_2))}{f_{Min}}$	1.22 MB
Asymmetric	$\frac{B \cdot F_{ADC}}{f_{Min}} \times \cdots$ $(P_3 V_2 A_3 L_2 + P_3 (A_3 + AP_4)(L_M - L_2) + A_3 L_M + D_2 L_M / 2)$	1.26MB

Where:
P_3=3 (3 phases of analysis)
P_2=2 (2 duplicated paths in the tick-tock architecture)
V_2=2 (a pair of real/imaginary values)
A_3=3 (3 buffers normally required for each averaging filter)
A_2=2 (2 buffers required for averaging within the tick-tock architecture)
AP_4=4 (4 buffers normally required to average phase)
AP_2=2 (2 buffers required for averaging phase within tick-tock architecture)
D_2=2 (2 buffers required to store and recall oscillator phase over half the filter length, accounting for phase wrapping, for the asymmetric method)
L_2=2 represents the 2-cycle long P class filter length.

In TABLE II, B is the number of bytes per sample, and f_{Min} is the minimum frequency at which the proposed filters will operate accurately. Examples, for the longest M class filter with F_S=10 Hz, F_{ADC}=10 kHz, 64-bit precision (B=8), f_0=60 Hz, and f_{Min}=45 Hz are given in the right hand column of TABLE II. The requirements of the larger M class algorithms preclude operation on the smallest microcontroller platforms, but operation on a real-time PC-based platforms such as the MVME5500 [35] presents no significant difficulty.

The algorithms they have been benchmarked on two different processors: the Infineon TC1796 [36], and the Motorola MVME5500. as described in [32], using the configurations described under TABLE II. The TC1796 used 32-bit whereas the MVME5500 used 64-bit arithmetic.

The proposed algorithms are much faster to execute than the Basic algorithms (TABLE III). This is due to the careful implementation of the averaging buffers [32], compared to the relatively long times required to compute the Basic FIR filter correlations. The proposed algorithms (in their entirety) support operation at sample rates in excess of 10 kHz

TABLE III
APPROXIMATE EXECUTION TIMES FOR P AND M CLASS PMUS

	Typical execution time per frame	
	TC1796	MVME5500
P Class Basic	710 µs	245 µs
P Class Symmetric "tick-tock"	54 µs	19 µs
P Class Asymmetric	41 µs	17 µs
M Class Basic	-	6200 µs
M Class Symmetric "tick-tock"	-	36 µs
M Class Asymmetric	-	30 µs

VI. SIMULATED PMU PERFORMANCE RESULTS

To test the proposed algorithms against the Basic algorithms, a 30 s test scenario is generated. This contains a variety of difficult signal conditions for the PMU algorithms to contend with. The scenario is described in TABLE IV. This is not formal testing to the C37.118 standard, although the test contains many sections which are designed to match the conditions laid down in the compliance sections of C37.118. These equivalent C37.118 tests are also shown in TABLE IV. It will be seen that there are several sections of the test which apply (realistic) test conditions which presently fall out-with the standard, for example unbalance, non-linear frequency ramps, higher frequency inter-harmonics, and multiple simultaneous harmonics. The frequency and positive sequence magnitude profile for this scenario is summarised in Fig. 9 and Fig. 10.

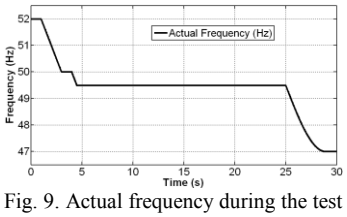

Fig. 9. Actual frequency during the test scenario

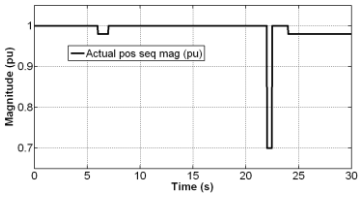

Fig. 10. Actual positive sequence magnitude during the test scenario

The sample rate used for the PMU algorithms is 10 kHz. A first-order 2.5kHz low-pass filter is modelled. A perfect 14-bit ADC is also modelled (as in [12]), which samples the signal over a ±2pu range so there are 13 effectively useful bits for a ±1pu nominal voltage signal.

To enable the easiest comparison of the results, between the different PMU designs, only the measurement errors (compared to the known generated signal) are presented in the figures below. Since the raw error plots can appear quite noisy, the errors are presented as unsigned magnitudes. The errors within ±½ of the allowed response times from each sudden signal change are also ignored (set to zero). The error datapoints are smoothed by taking the maximum of the nearest 11 errors in time (5 points either side), and assigning this maximum error to each report datapoint. The errors are then plotted on a logarithmic scale. These steps allow the errors from all three types of PMU design to be overlaid on the same graph and clearly distinguished.

TABLE IV
TEST SCENARIO

Time (s)		Signal	Equivalent C37.118 test
From	To		
-3	0	52 Hz balanced sinusoids, no harmonics (settling)	
0	1	52 Hz balanced sinusoids, no harmonics	Steady state, section 5.5.6. Off-nominal frequency.
1	3	Frequency ramp from 52-50 Hz at -1 Hz/s	Frequency ramp, section 5.5.7.
3	4	50 Hz balanced sinusoids, no harmonics	Steady State, section 5.5.6. Reference conditions.
4	4.5	Frequency ramp from 50-49.5 at -1 Hz/s	Frequency ramp, section 5.5.7.
4.5	6	49.5 Hz balanced sinusoids, no harmonics	Steady state, section 5.5.6. Off-nominal frequency.
6	7	Add unbalance (Negative sequence) 2% then remove	Outwith standard
7	8	Add 1% 5th harmonic (balanced) then remove	P class, Steady state, section 5.5.6. Off-nominal frequency with harmonic.
8	9	Add 10% 5th (balanced) then remove	M class, Steady state, section 5.5.6. Off-nominal frequency with harmonic.
9	10	Add 10% 5th (unbalanced) then remove.	Outwith standard
10	15	OOB (Out of band) signals (balanced), 10% amplitude, at 55, 65, 75, 85 & 95 Hz (1 second each) then remove	M class, Steady state, section 5.5.6. Off-nominal frequency with OOB interference.
15	20	OOB (balanced), 10% amplitude, at 3580, 3590, 3600, 3610 & 3620 Hz (1 second each) then remove	Outwith standard
21	21	Phase jump 20° at 21s	Dynamic compliance, section 5.5.8.
22	22.5	Dip Phase A (only) to 10% magnitude for ½ a second	Outwith standard
24	25	Add unbalance of 2% plus harmonics 2-40 at amplitudes allowed by Table 2 of EN 50160[18], scaled by 0.7016 to give an overall THD of 8%, with phases correlated for odd harmonics and random for even harmonics. Retain these additions for the remainder of the scenario.	Outwith standard
25	29	Frequency ramp from 49.5-47 Hz in a non-linear fashion, starting at -1 Hz/s	Outwith standard
29	30	Constant frequency of 47Hz	Steady state, section 5.5.6.

A. TVE performance

During the relevant parts of the test scenario for P class devices, even the simplest Basic P class PMU, is compliant with the TVE specification of ±1% (Fig. 11). Note that during the application of 10% OOB signals at 55-95 Hz (between t=10 s and t=15 s), the P-class devices are not required to be compliant. Actual high-amplitude signals at these frequencies are unlikely, and would violate flicker limits [18]. More likely are signals in the 9900-10100 Hz range which might alias (with F_{ADC} at 10kHz) into this region, but these will be at least partly attenuated by anti-aliasing filters. Another possibility is other inter-harmonic signals as applied between t=15 s and t=20 s. Even the P class PMU is shown to reject such signals at the 10% amplitude. In reality, high-frequency inter-harmonics at this 10% level are unlikely and equipment causing them would not be compliant.

The TVE performance of the M class PMUs (Fig. 12 ,F_S =50 Hz and Fig. 13, F_S=10 Hz) is also generally compliant. The F_S=50 Hz PMU is not required to be (and is not)

compliant to 1% TVE between t=10 s and t=12 s, since its filter cutoff frequency is 25 Hz. The Basic algorithm in this case is marginally not compliant for the 75 Hz OOB signal (t=12 s to t=13 s), but this could be remedied by slight adjustment of the filter length and cutoff frequency which were designed using generalised equations (7) & (9) rather than carefully tuning the filter for each F_S option or using Table C.1 of [13].

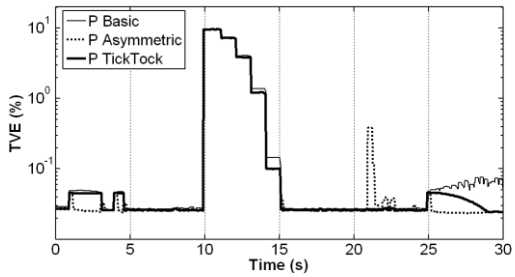

Fig. 11. TVE errors for P class devices.

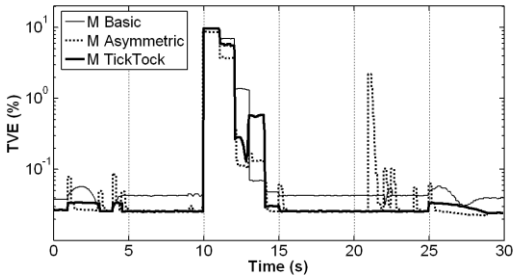

Fig. 12. TVE errors for M class devices (F_S=50 Hz)

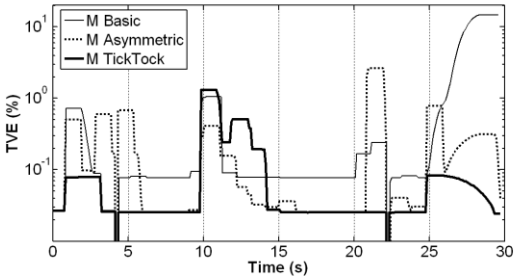

Fig. 13. TVE errors for M class devices (F_S=10 Hz)

The proposed M class TickTock algorithm is not quite so good at rejecting the OOB signals in the 75-85 Hz range (t=12 s to t=14 s) as the Basic algorithm, due to the filter response shown in Fig. 7b, but for higher frequency interfering signals the proposed algorithms provide much more attenuation than the Basic algorithm (Fig. 7c and Fig. 7d) and this leads to lower TVE levels than the Basic algorithm over most of the scenario, particularly when harmonics are present.

The TVE error of the F_S=10 Hz Basic algorithm rises significantly above 1% when the fundamental drops below 48 Hz at t>26 s, which is outside the required range in [13] but is an important frequency range since grid codes typically require generators to stay on-line until 47 Hz. It might be possible to reduce this error with a more complex amplitude calibration which extends into the attenuated part of the Basic filter response (Fig. 7a). However, another part of this error is the lack of calibration due to the frequency chirping effect, that also causes a phase error which is visible in the TVE error between t=1 s and t=3 s.

The TVE of the F_S=10 Hz Asymmetric algorithm is also slightly in error during the non-linear frequency ramp to 47 Hz at t>25 s, and the cause is not yet known. The frequency-chirp calibration (19) of the TickTick algorithm works very well even at F_S=10 Hz, despite the fact that ROCOF is deliberately not constant during this part of the test.

In general, with respect to TVE, for all but the largest and most unbelievable interfering signals (the close-in OOB signals), it is seen that the P-class PMU provides results which are so good that the benefit of the M class device might be questioned. The F_S=50 Hz M class device does provide a slightly reduced TVE, but it is notable that the difficulties of calibrating the output during frequency ramps actually makes the slowest F_S=10 Hz devices give less accurate and slower responding information than the faster PMUs during such events.

B. Frequency measurement performance

The measurement of frequency (Fig. 14 to Fig. 16) begins to highlight more significant problems with the Basic filters, and advantages of the proposed designs. Similarly to the TVE results, only the M class PMUs with the longest filters (F_S=10 Hz) are able to avoid spurious readings during high-level close-in OOB interference. In this condition (Fig. 16, t=10 s to t=13 s), the errors from the proposed algorithms are about 1/5th that of the Basic algorithm. Across the rest of the test duration, all devices perform generally within a ±0.01 Hz to ±0.02 Hz error. A significant exception is the Basic P-class algorithm (Fig. 14) when 8% THD is applied across many harmonics, coincidentally with unbalance and ROCOF at t=24 s to t=30 s. In this case, the frequency output becomes spurious to ±0.05 Hz, while the proposed algorithms give errors less than ±0.01 Hz.

The Basic M class devices with F_S=50 Hz (Fig. 15) also shows errors during this period which are not excessive (in the region of ±0.005 Hz/s) but are larger than the errors from the proposed algorithms.

The Asymmetric algorithm does show a tendency for the frequency measurement to "ring" following step changes in signal (e.g. t=1 s, 3 s, 4 s, 4.5 s etc), leading to some brief increases in signal error. After the input signal settles again, the Asymmetric algorithm can produce the best results, particularly for P class devices (Fig. 14).

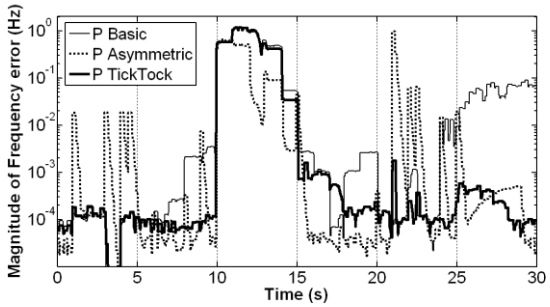

Fig. 14. Frequency errors for P class devices

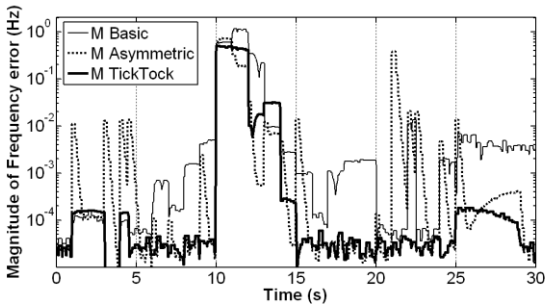

Fig. 15. Frequency errors for M class devices (F_S=50 Hz)

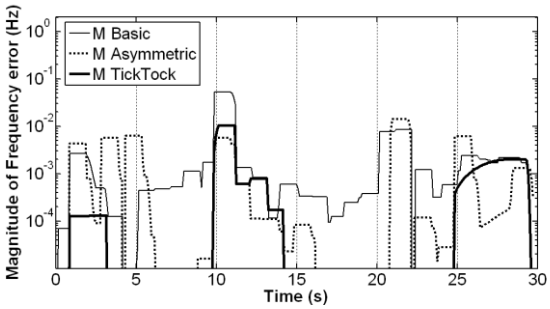

Fig. 16. Frequency errors for M class devices (F_S=10 Hz)

C. ROCOF measurement performance

Generally, the use of the Basic algorithm is found to give unsatisfactory ROCOF results across much of the test scenario. In P class (Fig. 17), the Basic algorithm can give a 0.00 Hz error between t=3 s and t=4 s (perfect 50 Hz signals, with ADC effects), but when frequency is offset to 49.5 Hz between t=4.5 s and t=6 s, the ROCOF errors are between 0.1 and 0.2 Hz/s. When the 1% harmonic is added, between t=7 s and t=8 s, the error rises to 0.4 Hz/s. Clearly this does not meet the standard which requires a 0.01 Hz/s accuracy. When the 10% harmonic (outside the scope of P class requirements) is added between t=8 s and t=9 s the error is 4 Hz/s. By comparison, the errors for the P class TickTock algorithm across these same scenarios is consistently <0.1 Hz/s. The performance of the P class Asymmetric algorithm shows some errors >0.1 Hz/s outside the allowed response time, due to the same ringing effect as described for the frequency measurement. However, once settled, the Asymmetric algorithm shows the lowest errors of all 3 algorithms at <0.01 Hz/s The Asymmetric algorithm would even be compliant to 0.01 Hz/s during the frequency ramp with 8% THD event between t=25.5 s and t=30 s.

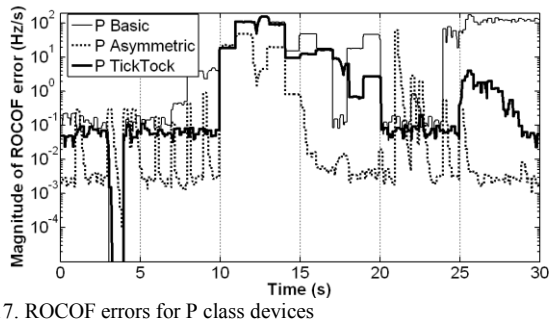

Fig. 17. ROCOF errors for P class devices

Between t=8 s and t=10 s, when a single 10% harmonic is applied, the Basic M class algorithms have errors of 3-6 Hz/s (F_S=50 Hz, Fig. 18) and 1-3 Hz/s (F_S=10 Hz, Fig. 19). The standard here is very wide and allows 6 Hz/s and 2 Hz/s respectively. This is due to the misalignment of the notches in the Basic filter. The proposed algorithms give errors <0.01 Hz/s.

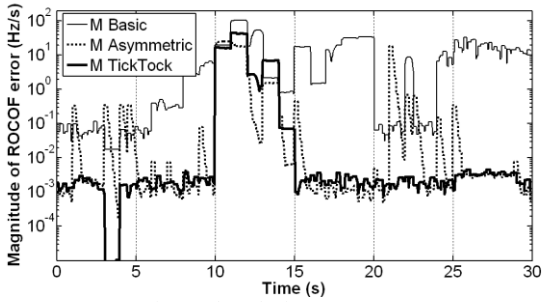

Fig. 18. ROCOF errors for M class devices (F_S=50 Hz)

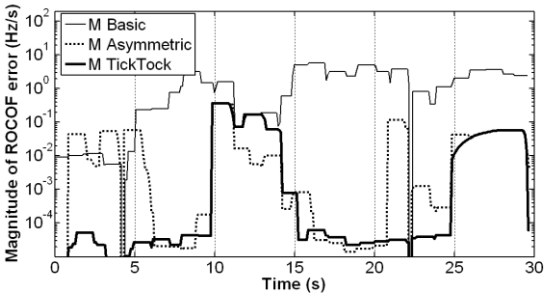

Fig. 19. ROCOF errors for M class devices (F_S=10 Hz)

Significant attention should be paid to the last few seconds of the scenario, between t=24 s and t=30 s, when a believable 8% THD is applied during a non-linear ROCOF event. The Basic P class device errors are in excess of 100 Hz/s (Fig. 17), and the Basic M class errors are >10 Hz/s and >2 Hz/s for the F_S=50 Hz and F_S=10 Hz devices respectively (Fig. 18 and Fig. 19). During the same parts of the scenario, the proposed algorithms show dramatically improved performance. The P class TickTock algorithm has errors of up to 2 Hz/s, but the other proposed variants have errors of only <0.01 Hz/s (P Asymmetric), <0.005 Hz/s (M class at F_S=50 Hz), and <0.1 Hz/s (M class at F_S=10 Hz). This last point is interesting because it confirms that, as first shown in the TVE measurements, longer measurement windows do not necessarily lead to better results during ROCOF events. In this case, the proposed M class PMUs with F_S=50 Hz produce the most accurate results.

All of the algorithms struggle to produce a useful ROCOF result during the worst OOB testing, although the errors from the proposed algorithms are smaller than those of the Basic algorithm. All the M class algorithms would fail to meet the OOB requirement (0.1 Hz/s), and it is not clear how this requirement could actually be met.

One possibility is that technically, Tables 10 and 11 in [13] allow Frequency and ROCOF measurements to have longer response times than the TVE measurements. This means that the Frequency and ROCOF measurements could be further filtered before being reported. This means that they should also be given a different timestamp to the TVE measurement, but the message format means that they must be given the

same timestamp [14] and misleading information would therefore be given to the PDC. In this paper, no such additional filtering is implemented and the TVE, frequency and ROCOF measurements are all given at the same timestamp, with a response time to meet TVE response specifications.

VII. Conclusions

In this paper we find that there appear to be some large mismatches between the requirements of the new PMU standard C37.118.1, and the algorithm which it suggests should be compliant. Alternative algorithms have been proposed which provide much better performance, particularly with respect to off-nominal frequency, ROCOF events, and harmonic contamination. The proposed algorithms have all been benchmarked and found to be viable at sample rates of 10kHz or more (being less computationally intensive than a traditional FIR filter), and can produce continuous reports at this rate if required.

In general, compliance with TVE is relatively easy, although care is required during high ROCOF events and new calibration techniques are demonstrated to deal with this. The proposed algorithms allow operation over much wider frequency ranges than the Basic algorithms, without additional difficulties in calibration of filters over wide ranges.

Meeting the frequency measurement requirement is more difficult, and the minimisation of ROCOF error is the most difficult thing to achieve. It is shown that minimising the ROCOF error is equally as important as minimising the TVE error if the PMU results are to be of any use at the PDC. The following points should be highlighted:

- The Basic P class algorithm cannot comply with the proposed 0.01 Hz ROCOF accuracy during off-nominal frequencies, even with no harmonic contamination. However, the proposed Asymmetric P class algorithm can (even with 8% THD across harmonics 2-40).
- Meeting the 0.1 Hz/s ROCOF accuracy for M class devices during OOB testing is very hard, and it is not clear how this will be achieved. However, it is also not clear how a 10% interfering signal will actually appear at the fundamental frequency ±5 Hz (which would violate flicker limits), and so the real-world relevance of the OOB tests are questioned. A more realistic test might be to apply interfering signals over a range, close to the sampling rate of the PMU, thereby validating both the anti-alias filter and digital filter performance.
- The requirement for M class devices to have ROCOF accuracies as wide as 2-6 Hz/s during 10% harmonic contamination seems to be far too loose to be useful at the PDC. While the Basic algorithm does give errors of this magnitude, it is shown that the proposed algorithms could meet a 0.01-0.1 Hz/s specification under the same conditions.

Overall, the proposed P class Asymmetric algorithm (at any reporting rate), and the proposed M class TickTock algorithm with a reporting rate of F_S=50 Hz are found to give the best results. It is found that the slower reporting rates such as F_S=10 Hz actually make TVE and ROCOF harder to measure accurately during dynamic events, and there is no noticeable benefit over the F_S=50 results unless close-in OOB performance is deemed to be a real issue. This risk can be minimised by operating the algorithms at high sample frequencies such as 10 kHz and applying sensible anti-alias filters which reduces the risk of aliased interference near the fundamental.

VIII. References

[1] R. Moxley and D. Dolezilek, "Case Studies: Synchrophasors for Wide-Area Monitoring, Protection, and Control," in *IEEE Innovative Smart Grid Technologies (ISGT) 2011*, Manchester, UK, 2011.

[2] M. G. Adamiak, A. P. Apostolov, M. M. Begovic, C. F. Heriville, K. E. Martin, G. L. Michel, A. G. Phadke, and J. S. Thorp, "Wide area protection - Technology and infrastructures," *IEEE Transactions on Power Delivery,* vol. 21, pp. 601-609, Apr 2006.

[3] A. Borghetti, C. A. Nucci, M. Paolone, G. Ciappi, and A. Solari, "Synchronized Phasors Monitoring During the Islanding Maneuver of an Active Distribution Network," *IEEE Transactions on Smart Grid,* vol. 2, pp. 82-91, 2011.

[4] J. Q. Tortós, G. Valverde, L. Ding, and V. Terzija, "Optimal Placement of Phasor Measurement Units to Improve Parallel Power System Restoration," in *IEEE Innovative Smart Grid Technologies (ISGT) 2011*, Manchester, UK, 2011.

[5] R. Lira, C. Mycock, D. Wilson, and H. Kang, "PMU Performance Requirements and Validation for Closed Loop Applications," in *IEEE Innovative Smart Grid Technologies (ISGT) 2011*, Manchester, UK, 2011.

[6] K. E. Martin, D. Hamai, M. G. Adamiak, S. Anderson, M. Begovic, G. Benmouyal, G. Brunello, J. Burger, J. Y. Cai, B. Dickerson, V. Gharpure, B. Kennedy, D. Karlsson, A. G. Phadke, J. Salj, V. Skendzic, J. Sperr, Y. Song, C. Huntley, B. Kasztenny, and E. Price, "Exploring the IEEE standard C37.118-2005 synchrophasors for power systems," *IEEE Transactions on Power Delivery,* vol. 23, pp. 1805-1811, Oct 2008.

[7] A. G. Phadke, J. S. Thorp, R. F. Nuqui, and M. Zhou, "Recent Developments in State Estimation with Phasor Measurements," *2009 IEEE/PES Power Systems Conference and Exposition, Vols 1-3,* pp. 1233-1239, 2009.

[8] J. Depablos, V. Centeno, A. G. Phadke, and M. Ingram, "Comparative testing of synchronized phasor measurement units," *2004 IEEE Power Engineering Society General Meeting, Vols 1 and 2,* pp. 948-954, 2004.

[9] G. Y. Yang, K. E. Martin, and J. Østergaard, "Investigation of PMU Performance Under TVE criterion," in *5th International Conference on Critical Infrastructure (CRIS)*, 2010.

[10] IEEE, "IEEE Standard for Synchrophasors for Power Systems," C37.118-2005, 2005.

[11] Y. Hu and D. Novosel, "Progresses in PMU testing and calibration," *2008 Third International Conference on Electric Utility Deregulation and Restructuring and Power Technologies, Vols 1-6,* pp. 150-155, 2008.

[12] M. Lixia, C. Muscas, and S. Sulis, "On the accuracy specifications of Phasor Measurement Units," *2010 IEEE International Instrumentation and Measurement Technology Conference I2mtc 2010, Proceedings,* 2010.

[13] IEEE, "IEEE Standard for Synchrophasor Measurements for Power Systems," C37.118.1-2011, 2011.

[14] IEEE, "IEEE Standard for Synchrophasor Data Transfer for Power Systems," C37.118.2-2011, 2011.

[15] EURAMET EMRP, "EMRP EURAMET Smart Grid Metrology," 2012 Available: http://www.smartgrid-metrology.eu/, accessed February 2012.

[16] A. J. Roscoe, I. F. Abdulhadi, and G. M. Burt, "P-Class Phasor Measurement Unit Algorithms Using Adaptive Filtering to Enhance

This is a slightly expanded postprint of a paper published in IEEE Transactions on Power Delivery [http://dx.doi.org/10.1109/TPWRD.2013.2238256] and is subject to IEEE copyright.

Accuracy at Off-Nominal Frequencies," in *IEEE SMFG 2011 Smart Measurements For Future Grids*, Bologna, Italy, 2011.
[17] D. Laverty, J. O'Raw, D. J. Morrow, M. Cregan, and R. Best, "Practical Evaluation of Telecoms for Smart Grid Anti-Islanding Protection," in *IEEE Innovative Smart Grid Technologies (ISGT) 2011*, Manchester, UK, 2011.
[18] CENELEC, "Voltage characteristics of electricity supplied by public distribution systems," EN 50160, 2000.
[19] A. G. Phadke and B. Kasztenny, "Synchronized Phasor and Frequency Measurement Under Transient Conditions," *IEEE Transactions on Power Delivery,* vol. 24, pp. 89-95, Jan 2009.
[20] M. H. Wang and Y. Z. Sun, "A practical method to improve phasor and power measurement accuracy of DFT algorithm," *IEEE Transactions on Power Delivery,* vol. 21, pp. 1054-1062, Jul 2006.
[21] M. Akke and J. S. Thorp, "Sample Value Adjustment Improves Phasor Estimation at Off-Nominal Frequencies," *IEEE Transactions on Power Delivery,* vol. 25, pp. 2255-2263, Oct 2010.
[22] D. Belega and D. Petri, "Accuracy of a DFT phasor estimator at off-nominal frequency in either steady state or transient conditions," in *IEEE SMFG 2011 Smart Measurements For Future Grids*, Bologna, Italy, 2011.
[23] H. S. Zhao, Z. Y. Liu, G. W. Song, and D. L. Wei, "The Analysis of Frequency Deviation on Synchrophasor Calculation and Correction Methods," *2009 International Conference on Sustainable Power Generation and Supply, Vols 1-4,* pp. 387-391, 2009.
[24] R. Petrella, A. Revelant, and P. Stocco, "Robust Grid Synchronisation in Three-Phase Distributed Power Generation Systems by Synchronous Reference Frame Pre-Filtering," in *Universities' Power Engineering Conference (UPEC)*, Glasgow, UK, 2009.
[25] H. Qian, R. X. Zhao, and T. Chen, "Interharmonics analysis based on interpolating windowed FFT algorithm," *IEEE Transactions on Power Delivery,* vol. 22, pp. 1064-1069, Apr 2007.
[26] G. W. Chang, C. I. Chen, Y. J. Liu, and M. C. Wu, "Measuring power system harmonics and interharmonics by an improved fast Fourier transform-based algorithm," *IET Generation Transmission & Distribution,* vol. 2, pp. 192-201, Mar 2008.
[27] A. J. Roscoe and G. M. Burt, "Comparisons of the Execution Times and Memory Requirements for High-speed Discrete Fourier Transforms and Fast Fourier Transforms, for the Measurement of AC Power harmonics," in *2nd IMEKO TC 11 International Symposium METROLOGICAL INFRASTRUCTURE*, Cavtat, Dubrovnik Riviera, Croatia, 2011.
[28] R. K. Mai, L. Fu, Z. Y. Dong, B. Kirby, and Z. Q. Bo, "An Adaptive Dynamic Phasor Estimator Considering DC Offset for PMU Applications," *IEEE Transactions on Power Delivery,* vol. 26, pp. 1744-1754, Jul 2011.
[29] T. Lin and A. Domijan, "Recursive algorithm for real-time measurement of electrical variables in power systems," *IEEE Transactions on Power Delivery,* vol. 21, pp. 15-22, Jan 2006.
[30] F. Muzi and M. Barbati, "A real-time harmonic monitoring aimed at improving smart grid power quality," in *IEEE SMFG 2011 Smart Measurements For Future Grids*, Bologna, Italy, 2011.
[31] A. J. Roscoe, G. M. Burt, and J. R. McDonald, "Frequency and fundamental signal measurement algorithms for distributed control and protection applications," *IET Generation, Transmission & Distribution* vol. 3, pp. 485-495, May 2009.
[32] A. J. Roscoe, S. M. Blair, and G. M. Burt, "Benchmarking and optimisation of Simulink code using Real-Time Workshop and Embedded Coder for inverter and microgrid control applications," in *UPEC: 2009 44th International Universities Power Engineering Conference*, 2009, pp. 532-536.
[33] A. J. Roscoe, R. Carter, A. Cruden, and G. M. Burt, "Fast-Responding Measurements of Power System Harmonics using Discrete and Fast Fourier Transforms with Low Spectral Leakage," in *1st IET Renewable Power Generation Conference*, Edinburgh, Scotland, 2011.
[34] A. J. Roscoe, I. F. Abdulhadi, and G. M. Burt, "Filters for M class Phasor Measurement Units," in *IEEE International workshop on Applied Measurements for Power Systems (AMPS)*, Aachen, Germany, 2012.
[35] Emerson Network Power, "MVME5500 VME with PowerPC Processor," Available: http://www.emersonnetworkpower.com, accessed January 2011.
[36] Infineon Technologies, "Infineon Tricore family (TC1796)," Available: http://www.infineon.com, accessed January 2011.

IX. BIOGRAPHIES

Andrew J. Roscoe received the B.A. and M.A. degree in Electrical and Information Sciences Tripos at Pembroke College, Cambridge, England in 1991 & 1994. Andrew worked for GEC Marconi from 1991 to 1995, where he was involved in antenna design and calibration, specialising in millimetre wave systems and solid state phased array radars. Andrew worked from 1995 to 2003 with Hewlett Packard and subsequently Agilent Technologies, in the field of microwave communication systems, specialising in the design of test and measurement systems for personal mobile and satellite communications. Andrew was awarded an MSc from the University of Strathclyde in 2003, in the field of "Energy systems and the Environment", and received his Ph.D degree in 2009. Andrew is currently a Lecturer in the Institute for Energy and the Environment, Department of Electronic and Electrical Engineering at Strathclyde University, working in the fields of distributed and renewable generation, active network management, power system metrology, inverter control, and marine/aero power systems.

Ibrahim F. Abdulhadi (S'08, M'11) received the MEng degree at the University of Strathclyde in 2007. He is currently a Research Assistant within the university's Institute for Energy and Environment and is working towards his PhD on adaptive power system protection. He has experiece working for UK distribution and transmission network operators. His current research interests include the application of PMUs for wide area protection, real-time power system simulation, hardware in the loop testing and communications applications in smart grids.

Prof. Graeme M. Burt (M'95) currently holds a chair in Power Systems within the Institute for Energy and Environment at the University of Strathclyde. He received his B.Eng. in Electrical and Electronic Engineering from the University of Strathclyde in 1988. His Ph.D. was awarded in 1992 by the University of Strathclyde following research into fault diagnostic techniques for power networks. He is currently the Director of the University Technology Centre in Electrical Power Systems sponsored by Rolls-Royce. His current research interests lie in the areas of: protection and control for distributed generation; power system modeling and simulation; and active distribution networks.